

# A FAST METHOD FOR COMPUTING AND CORRECTING INTENSITY INHOMOGENEITIES IN MRI

*Olivier Noterdaeme\* and Sir Michael Brady*

Wolfson Medical Vision Laboratory, University of Oxford, Oxford OX1 3PJ, UK

## ABSTRACT

In Magnetic Resonance Imaging (MRI) a given tissue may have quite different intensities depending on its location in the image volume. Such intensity inhomogeneities often arise from what is usually called the bias field, and are due to radio frequency inhomogeneities, variations in the static magnetic field and the distance of the tissue to the receiving coil. We present an efficient approach to determine such inhomogeneities from a series of calibration scans, which take less than 40 seconds to acquire. This enables us to efficiently correct both  $T_1$  and  $T_2$  weighted images. We present the theoretical background, as well as typical results for phantom, liver, pelvic and spine images.

**Index Terms**— Magnetic resonance imaging, Image enhancement, Image analysis, Biomedical image processing

## 1. INTRODUCTION

Ideal Magnetic Resonance Images (MRI) would associate with any given tissue a single intensity value. However, largely due to inhomogeneities in the static magnetic field, the radio frequency field and the variable distances of tissue to the receive coil, this is almost never the case. In clinical practice, we have observed variations of up to a factor of ten for a given tissue, for example in the case of spine images as shown in Figure 4(a), where the inhomogeneities are particularly severe.

Inhomogeneities particularly impact on contrast and can negatively challenge clinical decision making. Images are difficult to analyse at a single window/level setting, since areas can either be too dark or saturated. Intensity inhomogeneities can cause the intensity distribution of two distinct tissues to overlap. Image analysis algorithms, such as segmentation and registration techniques working on image intensities, are prone to failure. Intensity inhomogeneities become more pronounced at higher field strengths and there is a continued need for fast and accurate methods to correct for these inhomogeneities.

Previous approaches to remove the bias field can be classed into three main categories: phantom based, image based and physics based. Phantom based intensity correction estimate

the inhomogeneities with a uniform phantom and correct subsequent images with this estimate. However, as the inhomogeneities are different for each patient, ie. the inhomogeneities are dependent upon the loading of the system, it is not possible to accurately compensate for patient specific variations. Image based methods (eg. [1, 2]) are able to retrospectively correct images but they all embody general assumptions, for example about the shape and the smoothness of the inhomogeneities. Their performance depends strongly upon the initialization of the algorithm and they often take several minutes per image to run. Finally, physics and sequence based approaches attempt to estimate the bias field through a series of acquisitions. One example is the acquisition of a proton density weighted image [3] or two images acquired with minimal  $T_1$  effect (eg. [4, 5]). The drawback of this approach is the relatively long repetition time (TR) needed to reduce the  $T_1$  effect, which directly impacts on the duration of such calibration scans (several minutes). These approaches are hard to apply to abdominal imaging. For a more complete description of intensity correction techniques the reader is referred to one of the recent review papers on this topic [6, 7].

Our approach falls into the third category, ie. it is a sequence based approach. However, as we do not need to minimise any  $T_1$  effects we can choose a short TR and thus acquire the necessary information in <40 seconds. We are currently extending our method to combine it with image based techniques.

Our method uses a pair of object/patient specific calibration scans with varying flip angles to compute a spatially varying parameter that we call  $M_0(\vec{x})$ , where  $(\vec{x})$  is the pixel location. In most of the following, we suppress mention of  $\vec{x}$  since the method works independently at each location (though it does not have to be applied in this way). Our theoretical formulation indicates that under certain conditions  $M_0$  accurately represents the bias field,  $B$ , allowing us to correct any images acquired during the same exam. In our current implementation, we use a spoiled gradient recalled echo (SPGR) sequence with varying flip angle, such as the one from Deoni et al. [8]. However, the method is more generally applicable. Section 2 presents the theoretical background of the technique. In Section 3 we describe the imaging protocol and the results are shown in Section 4. Finally, Section 5 presents the Discussion and Conclusions.

\*This work is supported by General Electric Healthcare.

## 2. THEORY

Our method uses a series (a pair seems to suffice) of fast spoiled gradient echo (FSPGR) calibration images with different flip angles at the beginning of an MR exam, in order to compute  $M_0$ . As we will see, by choosing a very short echo time  $M_0$  effectively represents the bias field. The inhomogeneities in any image acquired during the same exam can then be corrected by dividing the acquired image by  $M_0$ . The FSPGR signal at any voxel is given by the signal equation

$$S^{\text{ideal}} = g\rho e^{-\text{TE}/T_2^*} \sin \alpha \left( \frac{1 - e^{-\text{TR}/T_1}}{1 - \cos \alpha \cdot e^{-\text{TR}/T_1}} \right) \quad (1)$$

The scanner gain  $g$ , repetition time TR, echo time TE and flip angle  $\alpha$  are sequence parameters that are independent of the voxel location. The tissue parameters such as the proton density  $\rho$ , longitudinal relaxation time  $T_1$  and the transverse relaxation time  $T_2^*$  are each functions of the spatial location  $\bar{x}$ . However, the signal is often contaminated by a bias field  $B(\bar{x})$ . This can be modeled as a multiplicative field [2], resulting in the observed Signal  $S^{\text{obs}}$ :

$$S^{\text{obs}} = g\rho e^{-\text{TE}/T_2^*} \sin \alpha \left( \frac{1 - e^{-\text{TR}/T_1}}{1 - \cos \alpha \cdot e^{-\text{TR}/T_1}} \right) B \quad (2)$$

which can be re-arranged to give

$$\frac{S^{\text{obs}}}{\sin \alpha} = \overbrace{e^{-\text{TR}/T_1}}^{E_1} \frac{S^{\text{obs}}}{\tan \alpha} + \overbrace{g\rho e^{-\text{TE}/T_2^*} B}^{M_0} \left( 1 - \overbrace{e^{-\text{TR}/T_1}}^{E_1} \right) \quad (3)$$

This is of the general form  $y = ax + b$ . By for example varying  $\alpha$ , while keeping all other sequence parameters constant, it is possible to estimate  $T_1$  and  $M_0$  by linear regression.

$$T_1 = -\frac{\text{TR}}{\ln a} \quad (4)$$

$$M_0 = \frac{b}{1 - a} \quad (5)$$

Note that the calculation of  $T_1$  is independent of the bias field. However, the calculation of  $M_0$  is corrupted by the bias field because  $M_0 = g\rho e^{-\text{TE}/T_2^*} B$ . However, when TE is short, as is often the case in practice, then Figure 1 confirms that for a range of realistic  $T_2^*$  values  $e^{-\text{TE}/T_2^*} \approx 1$  is a reasonable approximation. Under these circumstances, ie. short TE:

$$M_0 = g\rho e^{-\text{TE}/T_2^*} B \approx g\rho B \quad (6)$$

$M_0$  when computed from multiple FSPGR images with varying  $\alpha$  and short TE is corrupted by the bias field, but contains a negligible contribution from the transverse tissue relaxation time  $T_2^*$ .

Other images acquired during the same exam can then be corrected by dividing the acquired image with the computed  $M_0$ .

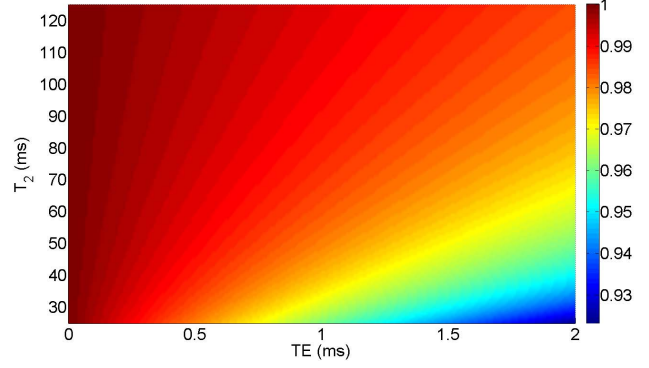


**Fig. 1.** Calculated  $e^{-\text{TE}/T_2^*}$  for a range of TE and  $T_2^*$ . For TE < 1.5msec the term  $e^{-\text{TE}/T_2^*}$  never drops below 0.95, making  $e^{-\text{TE}/T_2^*} \approx 1$  a reasonable assumption.

Object	Seq	Coil	acq matrix	TR/TE	$\alpha$
Phantom	$T_1$ GR	1	256x192	3.9/1.9	35
Phantom	$T_2$ SE	1	256x224	2000/96.6	90
Liver	$T_1$ GR	2	288x128	7.9/4.2	30
Liver	$T_2$ SE	2	256x224	2000/96.6	90
Rectum	$T_2$ SE	2	384x256	3700/92.1	90
Spine	$T_1$ SE	3	512x256	420/13.1	90

**Table 1.** Imaging sequences used.  $T_{1/2} = T_{1/2}$  weighted; GR=Gradient Echo; SE=Spin Echo and variations thereof. Coil 1 = General purpose Flex Coil (GE). Coil 2 = 8 Channel Phased Array Body Coil (GE). Coil 3 = 8 Channel Phased Array Cervical Thoracic Lumbar Spine Coil (USA Instruments).

## 3. METHODS AND MATERIALS

Images covering the entire object were acquired on a General Electric (GE) 1.5T system. We first acquired calibration images with DESPOT1 [8] at  $3^\circ$  and  $15^\circ$  using a 256x192 acquisition matrix, with TR/TE 3.4/1.2msec. The other sequences used in this paper are summarised in Table 1 and have been chosen as they are part of standard clinical protocols.  $M_0$  was computed from the calibration images and re-sliced, using linear interpolation, to the orientation and resolution of the images to be corrected. A large kernel median filter was applied to  $M_0$  to reduce noise. The original images were corrected by division with  $M_0$ . For comparison with our method, the spinal MR images were also corrected with GE Healthcare's PURE (Phased Array Uniformity Enhancement) technique and a local implementation of Styner's algorithm [1]. PURE uses a different type of calibration scan to correct for inhomogeneities.

## 4. RESULTS

Representative images before and after correction are shown in Figures 2, 3 and 4. Numerical results are given in Table 2.

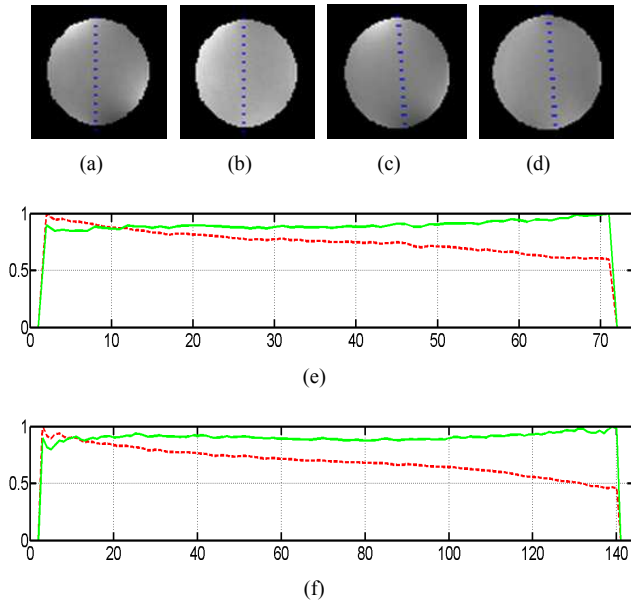


**Fig. 2.**  $T_1$  W image (a) before (red dashed) and (b) after (green solid) correction with corresponding line plot shown in (e). Analogous for a  $T_2$  W image, (b), (d) and (f). In both cases the corrected image, (b) and (d), demonstrates a more homogeneous appearance and the line plots resemble more closely the expected step function.

For phantom images, Figure 2, we show line plots of the intensities for the  $T_1$  and  $T_2$  weighted images before (dashed red) and after (solid green) correction. The corrected image consistently demonstrate a more homogeneous appearance, and the line plots show that the corrected image resembles more a step like function when compared to the line plot of the uncorrected image whose intensity gradually decreases.

Figure 3 shows that the technique successfully works for  $T_2$  weighted liver imaging. There is a significant reduction of intensity around the arrow, while there is an increase in intensity around the triangle, resulting in a more homogeneous appearance.

Finally, Figure 4 shows a sagittal  $T_1$  weighted image of the spine, which demonstrates strong intensity inhomogeneities as the receive coil is embedded in the table. The intensities of tissue in proximity to the table are much higher and there is a rapid fall off as the distance from the coil increases. Figure 4(a) shows the original image, while (c) shows the results after applying Styner’s algorithm. In (c) it is possible to see some more details around the head, rib bone (left arrow) and spine (middle arrow). Applying PURE to the original image results in further improvements around the spine and aorta (see middle arrow in 4(d)). However, in both cases large areas are still nearly invisible at the chosen display settings and the fat at the back (right arrow) still has a large range of intensity values. Using our technique (b) re-

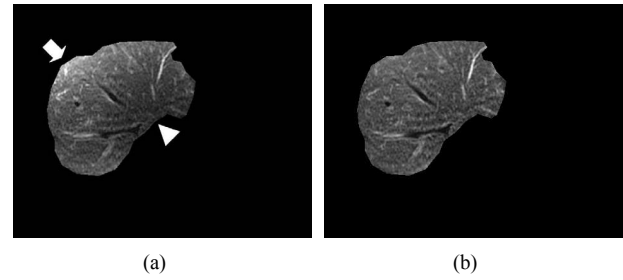


**Fig. 3.**  $T_2$  weighted liver image before and after correction using the new approach. The intensity is increased around the arrow and decreased around the triangle

Object	$\sigma/\mu$	$\sigma/\mu$ after correction
Phantom $T_1$ W	0.1562	0.1078
Phantom $T_2$ W	0.1576	0.0973
Liver $T_1$ W	0.2886	0.2140
Liver $T_2$ W	0.5692	0.3612
Rectum $T_2$ W	0.2093	0.1275
Spine $T_1$ W	0.2438	0.0951

**Table 2.** Standard deviation divided by the mean ( $\sigma/\mu$ ) of the signal intensities for homogeneous regions of interests for  $T_1$  and  $T_2$  weighted sequences. For every homogeneous tissue class a marked reduction in the parameter, consistent with the removal of bias field, is observed.

sults in a homogeneous image. Rib bone (left arrow), aorta and spine (middle arrow) and the fat (right arrow) can all be seen at the same time without loss of contrast between different tissue classes. The intensity of the fat at the back of the spine is very uniform from the top to the bottom of the image.

A numerical indication for the reduction in bias field is given by taking the standard deviation  $\sigma$  of a region and dividing by the mean  $\mu$  of the same region. For homogeneous regions the value of this parameter should be relatively small. A reduction in this parameter means that the histogram for this class becomes more narrow. Table 2 gives the numerical results for a number of different objects for  $T_1$  and  $T_2$  weighted sequences. Table 2 shows that  $\sigma/\mu$  after the application of our technique is in every case significantly smaller than on the original images, which is in agreement with the visual improvements observed.

## 5. DISCUSSION AND CONCLUSIONS

Table 1 and 2 show that we have successfully used our technique on numerous objects, sequences and coils. Obviously, the framework for the acquisition of our calibration images is in principle the same as the one used in the computation of the longitudinal relaxation time  $T_1$ . However, we highlight that with an appropriate choice of imaging parameters,  $M_0$

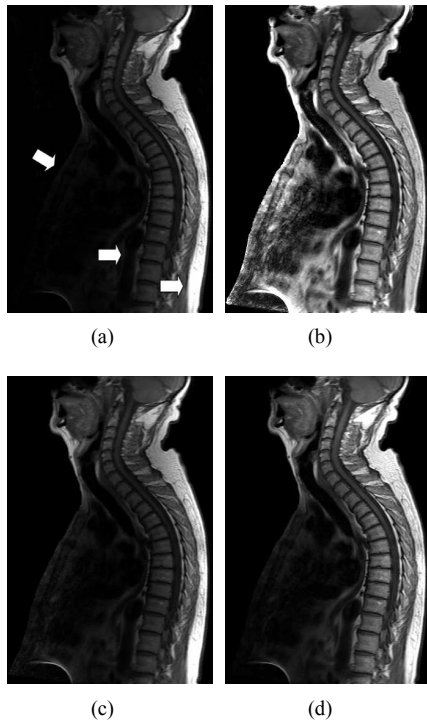


**Fig. 4.** (a) Original image and (b) after application of the approach described in Section 2, (c) Styner's algorithm and (d) PURE. Arrows point to some key areas.

can be used for intensity inhomogeneity correction. There are three main advantages of using  $M_0$  to correct intensity inhomogeneities over the reconstruction of synthetic images from parametric  $T_1$  maps (for an example of this see eg. [9]). Firstly, it is possible to correct both  $T_1$  and  $T_2$  weighted images. The reconstruction of synthetic images from parametric maps, requires high resolution  $T_1$  and  $T_2$  data, which require substantial imaging time. Secondly, as we are only interested in the shape of  $M_0$  we can easily deal with noise, eg. through median filtering or surface fitting. The computation of parametric images is a noisy process and reconstructing images from noisy raw data will result in noisy images. Thirdly, the shape of  $M_0$  can be obtained with a reduced image matrix, thereby offering further speed improvements.

We have presented a technique to remove inhomogeneities in MRI by computing  $M_0$  from a series of calibration images with varying flip angle. The short TR and the ability to reduce the imaging matrix enables the rapid acquisition of all calibration images ( $< 40$ seconds). We have shown that our technique successfully removes inhomogeneities on phantom, liver, pelvic and spine  $T_1$  and  $T_2$  weighted images acquired with a range of coils and that it outperforms existing techniques. In the future, we plan to integrate our approach with image based methods to further improve the performance of the algorithm by adding a suitable regulariser.

## 6. REFERENCES

- [1] M. Styner, C. Brechbuhler, G. Szekely, and G. Gerig, "Parametric estimate of intensity inhomogeneities applied to MRI," *IEEE Trans Med Imaging*, vol. 19, no. 3, pp. 153–65, 2000.
- [2] R. Guillemaud and M. Brady, "Estimating the bias field of MR images," *IEEE Trans Med Imaging*, vol. 16, no. 3, pp. 238–51, 1997.
- [3] G. P. Liney, L. W. Turnbull, and A. J. Knowles, "A simple method for the correction of endorectal surface coil inhomogeneity in prostate imaging," *J Magn Reson Imaging*, vol. 8, no. 4, pp. 994–7, 1998.
- [4] R. Stollberger and P. Wach, "Imaging of the active B1 field in vivo," *Magn Reson Med*, vol. 35, no. 2, pp. 246–51, 1996.
- [5] J. Wang, M. Qiu, Q. X. Yang, M. B. Smith, and R. T. Constable, "Measurement and correction of transmitter and receiver induced nonuniformities in vivo," *Magn Reson Med*, vol. 53, no. 2, pp. 408–17, 2005.
- [6] B. Belaroussi, J. Milles, S. Carne, Y. M. Zhu, and H. Benoit-Cattin, "Intensity non-uniformity correction in mri: existing methods and their validation," *Med Image Anal*, vol. 10, no. 2, pp. 234–46, 2006.
- [7] U. Vovk, F. Pernus, and B. Likar, "A review of methods for correction of intensity inhomogeneity in MRI," *IEEE Trans Med Imaging*, vol. 26, no. 3, pp. 405–21, 2007.
- [8] S. C. Deoni, B. K. Rutt, and T. M. Peters, "Rapid combined T1 and T2 mapping using gradient recalled acquisition in the steady state," *Magn Reson Med*, vol. 49, no. 3, pp. 515–26, 2003.
- [9] S. C. Deoni, B. K. Rutt, and T. M. Peters, "Synthetic T1-weighted brain image generation with incorporated coil intensity correction using DESPOT1," *Magn Reson Imaging*, vol. 24, no. 9, pp. 1241–8, 2006.